GNSS Signal Reliability Testing in Urban and Indoor Environments

Article · January 2004

CITATIONS
28

READS
1,031

2 authors:

Heidi Kuusniemi
Finnish Geospatial Research Institute
122 PUBLICATIONS **2,729** CITATIONS
SEE PROFILE

Gérard Lachapelle
The University of Calgary
107 PUBLICATIONS **1,911** CITATIONS
SEE PROFILE

GNSS Signal Reliability Testing in Urban and Indoor Environments

Heidi Kuusniemi*, Gérard Lachapelle
Department of Geomatics Engineering, University of Calgary, Canada

BIOGRAPHIES

Heidi Kuusniemi (born Sandström) received her MSc. degree in January 2002 from Tampere University of Technology, Finland, majoring in mathematics. Since then she has been continuing her studies as a PhD student at Tampere University of Technology. Currently, she is a visiting PhD student at the University of Calgary, in the Department of Geomatics Engineering.

Dr. Gérard Lachapelle holds a CRC/iCORE Chair in Wireless Location in the Department of Geomatics Engineering. He has been involved with GPS developments and applications since 1980 and has authored/co-authored numerous related publications and software. More information is available on http://PLAN.geomatics.ucalgary.ca

ABSTRACT

The availability of two GNSS (Global Navigation Satellite System), GPS and Galileo, will offer in future new possibilities to provide integrity and reliability information to the user both at signal and user levels due to increased redundancy. User-level reliability monitoring schemes, namely Receiver Autonomous Integrity Monitoring (RAIM), consist of statistically testing least-squares residuals of the observations on an epoch-by-epoch basis aiming towards reliable navigation fault detection and exclusion (FDE). Classic RAIM and FDE techniques are based on only GPS characteristics, so in this paper, methods will be discussed also suitable for a combined GPS/Galileo system with the focus on personal location in degraded signal environments.

This paper concentrates on analyzing different navigation quality and reliability assessment procedures based on testing the GNSS least-squares residuals on an epoch-by-epoch basis. The focus will be on reliability testing schemes for degraded GNSS signals in urban conditions in order to obtain an acceptable position estimate, and analyzing the urban GNSS navigation accuracy conditions. The reliability testing schemes for integrated GPS/Galileo to be discussed include applying a global test for detecting an inconsistent location situation, a local test for localizing and eliminating measurement errors recursively and, in addition, certain measurement subset testing. The proposed FDE schemes are examined with simulated GPS/Galileo data and real-life urban GPS tests. Furthermore, some external reliability measures, Mean Radial Spherical Error and Distance Root Mean Squared estimates approximating the effect measurement errors have on the accuracy will be analyzed.

This paper will provide an insight into user-level integrity and reliability monitoring and FDE schemes eligible for a future GNSS system particularly for degraded signal environments, where the conventional assumption of normally distributed errors does not necessarily hold. The aim is to improve solution reliability and provide additional accuracy information to the user in terms of approximated position error estimates.

INTRODUCTION

Location based services, the E911 and E112 mandates in the United States and Europe respectively, and personal and vehicular location and navigation applications call for capability also in degraded signal environments such as in urban areas and indoors. An urban environment places many challenges for satellite navigation due to, e.g., high buildings causing deterioration and total blockages to the satellite signals. Therefore, when using GPS alone in difficult positioning environments, there are unfortunately rarely enough satellite signals available for reliable position calculation. In future, the European navigation system Galileo will enhance significantly the positioning capability also in urban environments, and having access to two independent GNSS will most likely provide many advantages in availability, integrity, accuracy, and reliability, also for personal positioning in extreme signal masking environments.

Despite the increasing number of available satellites resulting from GPS/Galileo combination, it is evident that in urban areas and indoors, high-sensitivity processing is necessary to ensure sufficient signal availability. With high-sensitivity processing, however, the surroundings cause attenuation, deterioration, and multipath propagation on the received satellite signals. Thus, these severe interference effects lead to large measurement errors, and reliability monitoring is essential.

* **Visiting PhD student from Tampere University of Technology, Finland**

The simplest and lowest cost alternative in future to provide integrity and reliability information to the user will probably be to provide URA/SISA (User Range Accuracy/Signal in Space Accuracy) information at the signal level and complement this with RAIM, i.e., statistical reliability testing techniques, at the user level. Reliability monitoring consists of testing least-squares residuals of the observations for example on an epoch-by-epoch basis aiming towards navigation fault detection and exclusion. Classic RAIM techniques (Brown 1992, Ober 2003) aiming at fault isolation (Van Graas et al 1993) are based on only GPS characteristics, so in this research, methods will be discussed that are also suitable for combined GPS/Galileo. An exact generalization of the existing RAIM techniques is not efficient enough since it would lead to a high computational time of the user-level integrity monitoring process (Romay Merino et al 2001). Furthermore, the problem of multiple simultaneous signal failures can easily occur in difficult positioning environments requiring thus special attention.

When redundant observations have been made, the resulting residuals can be used to test the internal consistency among the obtained measurements. In this research, the reliability testing schemes for integrated GPS/Galileo include applying a global test for detecting an inconsistent navigation situation, a local test for localizing and eliminating measurement errors recursively and, in addition, certain subset testing for finding an acceptable subset of measurements. The FDE schemes are tested and examined with simulated GPS/Galileo data taking into account the multiple blunder situations, and with urban/indoor GPS tests with a high-sensitivity receiver. Furthermore, external reliability measures in terms of the effect that measurement errors have on the position accuracy will be estimated and examined.

The first section of the paper introduces internal and external reliability in navigation, discusses different FDE schemes implemented, and proposes measures to be used in evaluating the accuracy of a navigation situation in urban environments. The second section presents results and analyses of the implemented FDE schemes and reliability measures on simulated GPS/Galileo data and real HSGPS urban tests. Finally, conclusions are made with remarks on future work.

GNSS RELIABILITY

Introduction

The GNSS linearized measurement equations in least-squares epoch-by-epoch positioning can be expressed as follows (Kaplan 1996, Parkinson et al 1996)

$$\Delta\boldsymbol{\rho} = \mathbf{H}\Delta\hat{\mathbf{x}} + \boldsymbol{\varepsilon} \tag{1}$$

where $\Delta\boldsymbol{\rho}$ is the misclosure vector, that is, the difference between the predicted and measured pseudorange measurements, $\boldsymbol{\varepsilon}$ is the vector containing pseudorange measurement errors assumed to be normally distributed with zero-mean, that is, $\varepsilon_i \sim N(0,\sigma_i^2)$, and the matrix $\mathbf{H}$ is the geometry or design matrix. The epoch-by-epoch least squares positioning was used in this research instead of more practical filtering due to sensitivity analysis purposes. The incremental component from the linearization point, $\Delta\hat{\mathbf{x}}$, can be estimated as follows

$$\Delta\hat{\mathbf{x}} = \left(\mathbf{H}^{\mathbf{T}}\mathbf{C}_{\mathbf{l}}^{-\mathbf{1}}\mathbf{H}\right)^{-1}\mathbf{H}^{\mathbf{T}}\mathbf{C}_{\mathbf{l}}^{-\mathbf{1}}\Delta\boldsymbol{\rho} \tag{2}$$

where the matrix $\mathbf{C_l}$ is the covariance matrix of the measurements assumed here to be diagonal.

$$\hat{\mathbf{x}} = \mathbf{x_0} + \Delta\hat{\mathbf{x}} \tag{3}$$

Thus, the state estimate of the unknown user coordinates, i.e. $\hat{\mathbf{x}}$, can be obtained by adding the incremental component to an approximate component, i.e. a linearization point $\mathbf{x_0}$, as described in Eq. 3. This is conducted iteratively until the norm of the incremental value is small enough for the estimate $\hat{\mathbf{x}}$ to be accepted.

If redundant observations have been made, least-squares residuals can be obtained from least-squares estimation as follows (Ryan 2002, Wieser 2001)

$$\hat{\mathbf{r}} = \mathbf{H}\Delta\hat{\mathbf{x}} - \Delta\boldsymbol{\rho} = -\mathbf{C}_{\hat{\mathbf{r}}}\mathbf{C}_{\mathbf{l}}^{-\mathbf{1}}\Delta\boldsymbol{\rho}$$

where (4)

$$\mathbf{C}_{\hat{\mathbf{r}}} = \mathbf{C_l} - \mathbf{H}(\mathbf{H}^{\mathbf{T}}\mathbf{C}_{\mathbf{l}}^{-\mathbf{1}}\mathbf{H})^{-\mathbf{1}}\mathbf{H}^{\mathbf{T}}$$

The resulting residual vector $\hat{\mathbf{r}}$ can be used to test the internal consistency among the measurements (Kuang 1996). The residuals can be standardized/studentized as follows (Ryan 2002, Kelly, 1998)

$$w_i = \left| \frac{\hat{\mathbf{r}}_i}{\sqrt{(\mathbf{C}_{\hat{\mathbf{r}}})_{ii}}} \right| \quad , i = 1:n \tag{5}$$

where n denotes the number of observations.

Internal and External Reliability

Reliability refers to the controllability of observations, i.e., the ability to detect blunders and to estimate the effects that undetected blunders may have on the position solution (Leick 1995). Internal reliability quantifies the blunder that can be detected on each measurement through statistical reliability testing of least-squares residuals on an epoch-by-epoch basis. The smallest such blunder that can be detected is called the marginally, or minimum, detectable blunder (MDB). The external reliability is quantified by the size of the error in the navigation solution that is caused by the MDB (Kuang 1996, Ryan 2002, Petovello 2003).

The MDBs computed for all observations are measures of the capability to detect a blunder with the probability $(1-\beta_0)$ with $(1-\alpha_0)$ percent of confidence with the underlying assumptions including the presence of only one blunder at a time and a diagonal measurement covariance matrix, $\mathbf{C_l}$. Thus, given the probability levels α_0 and β_0 representing the false alarm rate and probability

of missed detection, respectively, the MDB for observation *i* is

$$MDB_i = \frac{\lambda_0 * (\mathbf{C_l})_{ii}}{\sqrt{(\mathbf{C_{\hat{r}}})_{ii}}} \quad (6)$$

where λ_0 is the non-centrality parameter of normal distributions as shown in Fig. 1 and presented as follows

$$\lambda_0 = n_{1-\frac{\alpha_0}{2}} + n_{1-\beta_0} \quad (7)$$

The effect of an undetected MDB on the estimated parameters is described by the observation external reliability. External reliability (ER) describing the effect a marginally detectable blunder in the i^{th} measurement has on the state estimate can be expressed as follows

$$\mathbf{ER}_i = -\left(\mathbf{H}^T\mathbf{C_l}^{-1}\mathbf{H}\right)^{-1}\mathbf{H}^T\mathbf{C_l}^{-1}\mathbf{MDB}_i \quad (8)$$

where the vector $\mathbf{MDB}_i$ is a column vector containing all zeros except for the MDB of the i^{th} observation in the i^{th} position (Ryan 2002). The external reliability represents the position error that is caused by the MDB.

$$TPE_i = \sqrt{\Delta\varphi_i^{\,2} + \Delta\lambda_i^{\,2} + \Delta h_i^{\,2}} \quad (9)$$

Thus, a total positioning error, TPE, can be defined that represents the 3D position error in latitude, longitude and height (Eq. 9), which the system can marginally be protected against for the given α_0 and β_0 values if the underlying assumptions are true and blunder detection presented later is being employed correctly.

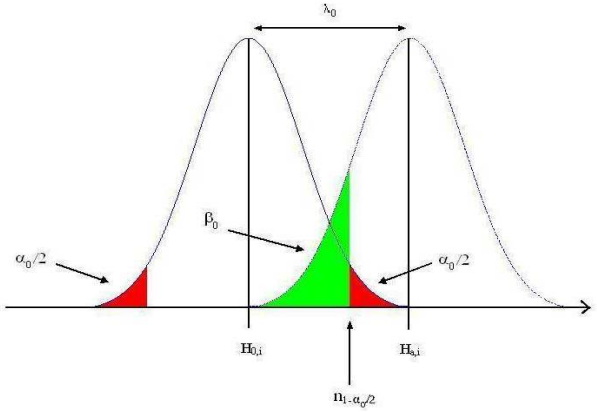

Figure 1 Normal distributions of standardized residuals in unbiased and biased cases

Statistical Reliability Testing (RAIM)

In order to detect a measurement error in the navigation situation using the least-squares position estimation approach, the least-squares residuals should be statistically tested. The errors in the linearized model are assumed Gaussian zero-mean in the unbiased case, which is unfortunately not necessarily true in degraded signal environments. Thus, the reliability theory for the FDE schemes to be presented does not necessarily hold for poor signal conditions, and precaution and special attention should be taken when interpreting the RAIM results.

A global test for detecting an erroneous and inconsistent navigation situation includes testing whether or not an 'a posteriori' variance factor, $\hat{\sigma}_0^2$, multiplied by the degrees of freedom (*n-p*) is centrally chi-squared distributed with a significance level of α and (*n-p*) degrees of freedom as presented in the following

$$\hat{\sigma}_0^2 = \frac{\hat{\mathbf{r}}^T\mathbf{C_l}^{-1}\hat{\mathbf{r}}}{n-p} \quad (10)$$

$$\hat{\sigma}_{0,threshold}^2 = \frac{\chi^2_{\alpha,n-p}}{n-p}$$

$$\begin{aligned} &H_0 : \hat{\sigma}_0^2 < \hat{\sigma}_{0,threshold}^2 \quad \text{(No integrity failure)} \\ &H_a : \hat{\sigma}_0^2 \geq \hat{\sigma}_{0,threshold}^2 \quad \text{(Integrity failure)} \end{aligned} \quad (11)$$

The parameter *n* denotes the number of satellites in view and the parameter *p* denotes the number of parameters to be estimated. Fig. 2 presents the central and non-central chi-square density functions that represent the null hypothesis and the alternative hypothesis for the global consistency test. This example is performed with eight degrees of freedom (*n-p*). The value α represents the significance level of the global test, i.e. the false alarm rate, the value β represents the probability of missed detection (Caspary 1988, Kuang 1996, Gertler 1998), and the value λ is the non-centrality parameter. The chi-square threshold $\chi^2_{\alpha,n-p}$ determines whether the null hypothesis of the global test is accepted or rejected. If the global test fails, i.e., the null hypothesis H_0 must be rejected and H_a accepted according to Eq. 11, inconsistency is assumed to occur in the measurements, and some action should be taken in terms of attempting to identify the measurement errors.

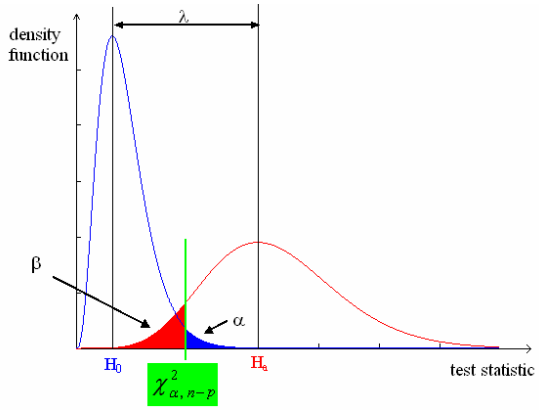

Figure 2 Central and non-central chi-square density functions for eight degrees of freedom

In case the global test fails, an attempt to correct the faulty navigation situation may be performed. With the assumption that only one blunder exists at a time, to detect that blunder, each standardized residual w_i presented in Eq. 5 can be statistically tested with a null hypothesis $H_{0,i}$, which represents the situation where the i^{th} residual is unbiased, against an alternative hypothesis

$H_{a,i}$, which represents the case where the i^{th} residual is biased. The underlying assumption is that the standardized residuals are normally distributed (Ryan 2002) with zero expectation in the unbiased case (Kuang 1996). The local test, i.e. the testing of the standardized residuals statistically to detect an outlier, is conducted as follows

$$\begin{aligned} H_{0,i} &: w_i < n_{1-\frac{\alpha_0}{2}} \quad (i \text{ acceptable}) \\ H_{a,i} &: w_i \geq n_{1-\frac{\alpha_0}{2}} \quad (i \text{ erroneous}) \end{aligned} \tag{12}$$

The measurement with the largest standardized residual exceeding the threshold is regarded as an outlier and that measurement is excluded from the navigation solution (Kelly 1998, Teunissen 1998). Thus, the k^{th} observation is suspected to be erroneous when

$$w_k \geq w_i \ \forall i \quad \wedge \quad w_k \geq n_{1-\frac{\alpha_0}{2}} \tag{13}$$

The local test is a single fault isolation test and resembles with the same threshold and performance criteria selections the fault detection and identification part of Kelly's integrity monitoring scheme (Kelly 1998). This scheme, the Maximum Residual Algorithm, includes also the assumption of only one satellite channel failure. Unfortunately, the assumption of a single blunder is not always valid, especially in urban environments. Thus, as an approximation for a testing procedure to detect multiple blunders, the single blunder local test may recursively be applied whenever a blunder is detected. If an outlier is found and excluded, the test is repeated on the subsample remaining after deletion of the outlier (Hawkins 1980, Petovello 2003). The exclusion of measurements based on the standardized residuals is performed sequentially until no more outliers are found in the navigation situation (Fig 3.).

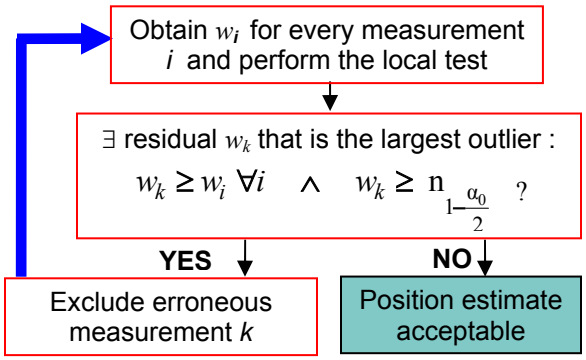

Figure 3 The sequential local test

The global and local consistency tests (Kuang 1996, Caspary 1988) are a part of a statistical reliability testing/outlier detection procedure introduced originally by Baarda (1968). If the global test fails, that is if the condition H_a is accepted, the local test is carried out. The risk level α of the global test relates to that of the local test, α_0, together with the β_0 value and the degree of freedom, n-p, in a way that the non-centrality parameter must be the same for both tests as expressed symbolically as follows (Caspary 1988)

$$\beta = \beta_0 \ , \lambda_0 = \lambda\,(\alpha_0, \beta_0, 1) = \lambda\,(\alpha, \beta_0, n-p) \tag{14}$$

The α value, when setting the α_0 and β_0 values, is obtained with the following procedure

$$\begin{aligned} \lambda = \lambda_0{}^2 &= (n_{1-\frac{\alpha_0}{2}} + n_{1-\beta_0})^2 \\ \chi^2_{(\beta_0,\, n-p,\, \lambda)} &= \chi^2_{(1-\alpha,\, n-p)} \Rightarrow \alpha \end{aligned} \tag{15}$$

Fault Detection and Exclusion Schemes

The outlier detection and identification strategy where the exclusion is based on the global and sequential local tests is presented as a flow chart in Fig. 4 and denoted later as the 'FDE A' procedure. After obtaining the measurements, the global test is conducted to find out the status of the navigation situation. If the global test does not pass, i.e., there is some inconsistency in the navigation solution, the local testing is performed and erroneous measurements are recursively excluded.

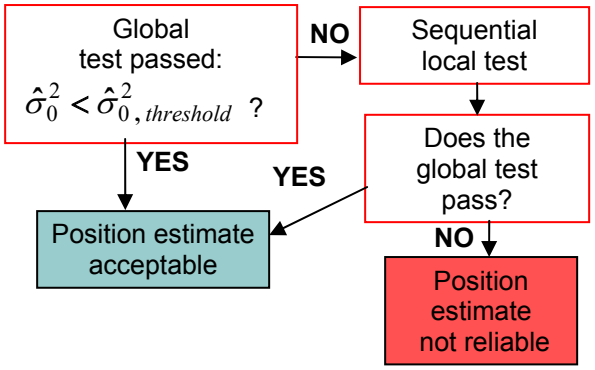

Figure 4 FDE scheme based on global and sequential local tests ('FDE A')

Unfortunately, the strategy presented in the above figure is suitable mainly for single fault situations, since the least-squares procedure tends to spread a blunder and particularly many blunders into all the residuals. Hence, wrong measurements might be marked to be erroneous in the recursive local test, especially in large or multiple bias situations (Lu 1991). Another procedure for multiple bias situations is thus needed apart from the sheer sequential local testing. Particularly, in epoch-by-epoch position calculation under degraded signal environments such as indoors, every available measurement is vital to the solution geometry. Thus, in some cases, including an erroneous measurement into the position solution might be a better alternative in terms of ensuring acceptable observation geometry than excluding that measurement. Thus, if excluding a measurement with a supposed blunder would lead to a poor HDOP (Horizontal Dilution of Precision) value, that measurement should not be

excluded, and the position solution obtained with the measurements at hand should be provided to the user, albeit with a warning (Lachapelle et al 2003).

Along with the FDE schemes based on sequential local testing, subset testing with the 'a posteriori' variance factor as the test statistic may be conducted to find a subset from which the supposed blunders are excluded. This is done by searching for a subset that most clearly passes the global test, i.e., which satisfies its self-consistency test with the smallest 'a posteriori' variance factor. In subset testing, the 'a posteriori' variance factors are computed for all the possible subsets that include five to n-1 measurements, i.e., from which n-5 to one observation has been excluded. The subset that has the smallest acceptable 'a posteriori' variance factor and, in addition, the largest number of measurements is then chosen to provide the best position solution as described in Fig. 5. The most acceptable subset that also has the maximum number of measurements is chosen by comparing the 'a posteriori' variance factor to the subset 'a posteriori' variance threshold $\hat{\sigma}^2_{0,threshold}(k)$, where k denotes the number of measurements in the subset.

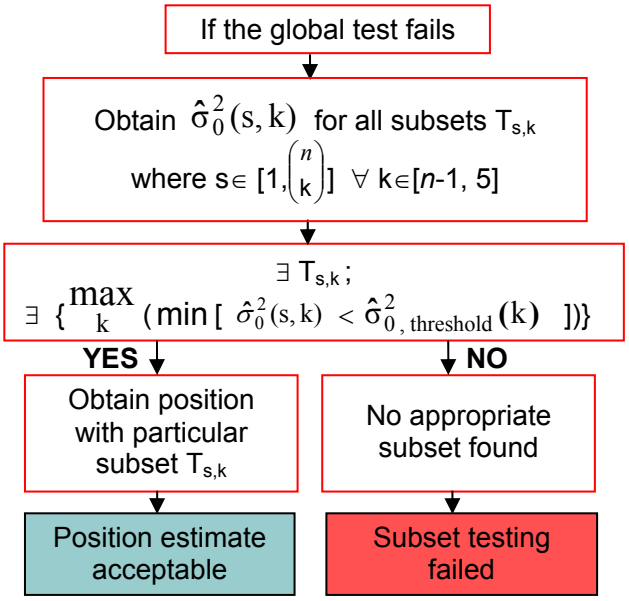

Figure 5 Subset testing FDE procedure

In addition to the subset testing procedure for avoiding unnecessary exclusions, another FDE scheme is also proposed consisting of the global and sequential local tests with possible back-implementation of already excluded measurements. Back-implementation is carried out if the global test passes when including an already excluded measurement as presented in Fig. 6. This FDE scheme is denoted later as the 'FDE B' procedure. Compared to the computationally heavy subset testing FDE, the 'FDE B' procedure has a significantly reduced computational burden.

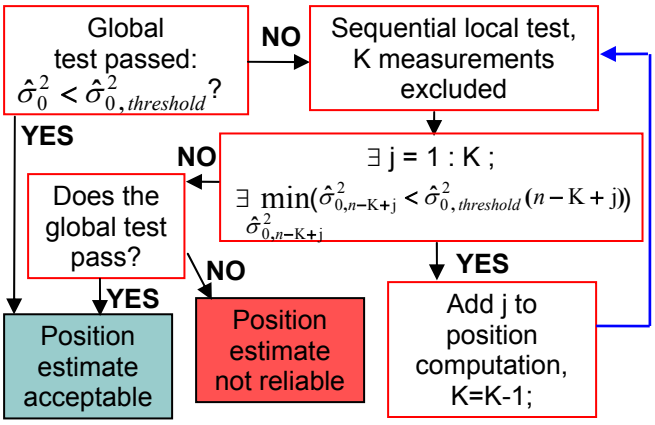

Figure 6 FDE with global and sequential local tests with back-implementation of excluded measurement to avoid unnecessary exclusions ('FDE B')

In the tests with the presented FDE schemes, the reliability testing parameters were set as follows for obtaining the global and local test thresholds

$$\left.\begin{aligned} \alpha_0 &= 0.1\% \;\Rightarrow\; n_{1-\alpha_0/2} = 3.29 \\ \beta_0 &= \beta = 10\% \Rightarrow \alpha\,(n-p) \;\Rightarrow\; \chi^2_{\alpha,n-p} \end{aligned}\right\} \qquad (16)$$

With these settings, as an example, when n-p = 10, the value α = 4.6%. If α_0 is increased, the local test threshold $n_{1-\alpha_0/2}$ is decreased leading to more exclusions, i.e. more good measurements are being allowed to be excluded, in the local test. In addition, a higher β_0 value will allow more erroneous measurements to be regarded as error-free, i.e. higher probability of missed detection. Overall, the α and β values specify, that in the presence of a blunder, the blunder can be detected with the probability of (1-β), with (1-α) percent of confidence.

Estimated accuracy measures of GNSS

Estimates of the accuracy and reliability of the user parameters can be obtained when multiplying the 'a posteriori' variance factor with the covariance matrix of the estimated user parameters resulting in distance root mean squared (DRMS) and mean radial spherical error (MRSE) estimates (Leick 1995).

$$\hat{\mathbf{C}}_{\hat{\mathbf{x}}} = \hat{\sigma}^2_0(\mathbf{H}^T\mathbf{C}_l^{-1}\mathbf{H})^{-1} = \begin{bmatrix} \hat{\sigma}^2_N & \hat{\sigma}_{NE} & \hat{\sigma}_{NU} \\ \hat{\sigma}_{NE} & \hat{\sigma}^2_E & \hat{\sigma}_{EU} \\ \hat{\sigma}_{NU} & \hat{\sigma}_{EU} & \hat{\sigma}^2_U \end{bmatrix} \qquad (17)$$

$$\hat{DRMS} = \sqrt{\hat{\sigma}^2_N + \hat{\sigma}^2_E} \qquad (18)$$

(2 * DRMS contains ~ 95 to 98% probability)

$$\hat{MRSE} = \sqrt{\hat{\sigma}^2_N + \hat{\sigma}^2_E + \hat{\sigma}^2_U} \qquad (19)$$

(1.56 * MRSE contains ~ 95% probability)

The estimates presented in Equations 18 and 19 can be used to assess the trustworthiness and accuracy of the obtained solution. Overall, the covariance matrix of the estimated unknowns multiplied by the 'a posteriori' variance factor (Eq. 17) estimates the accuracy of the estimated parameters and their correlation

SIMULATION TESTS WITH GPS/GALILEO

Standalone GPS in difficult positioning environments provides rarely sufficient satellite signal availability, i.e. enough redundancy, for reliable position calculation. Future Galileo will provide twice the number of satellites above the horizon (Ryan et al 2000, Weber et al 2001). With GPS/Galileo, better availability, accuracy, and reliability are expected, even in extreme masking environments (e.g. urban canyons) (O'Keefe 2001, Malicorne et al 2001). However, in harsh environments, signals are degraded which implies still a considerable need for reliability monitoring. Since no Galileo satellites or signal hardware simulators are available yet, a software simulator is a useful tool to assess the combined GPS/Galileo constellation and to check the usefulness of the proposed GNSS reliability testing algorithms for degraded signal environments.

A GNSS software simulator, SimGNSS2, developed by the PLAN group in the Department of Geomatics Engineering, University of Calgary, is used here for testing purposes of the FDE schemes. In generating the GNSS measurement scenarios, the simulator first computes the true observables (ranges and carrier phase) between the receiver and each GNSS satellite in-view. It then adds errors that affect the signals, with five different error factors being modeled: orbital uncertainties, ionospheric and tropospheric errors, as well as single-reflector multipath and receiver noise (Luo & Lachapelle 2003). The assumed GPS/Galileo constellation shown in Fig. 7 consists of 24+5 GPS satellites on 22000-km-radius circular orbits with an inclination angle of 55°, and 27+3 Galileo satellites on 29378-km-radius circular orbits with an inclination angle of 54° (Alves 2001).

In the simulated tests, only two frequencies, L1 and E1, were considered, a wide receiver correlator spacing was assumed, and an antenna height of 50 metres was set. The first test was performed by implementing artificial errors to an 'error-free' GPS/Galileo scenario and assessing the detection and exclusion capabilities of the presented FDE schemes and the resulting accuracies. Secondly, a data scenario of GPS/Galileo measurements with errors was generated and the performance of the FDE schemes was then assessed. When processing the simulated GNSS data with epoch-by-epoch least-squares estimation (a modified version of the University of Calgary C^{3}NAVG^{2TM} software package), the measurement variances were assumed equal to GPS and Galileo signals (a one-sigma value of approximately 4 m). Both of the simulated GNSS data sets were set to Calgary coordinates (51°, -114°, 1000 m) with a mask angle of 2° at GPS week 1248.

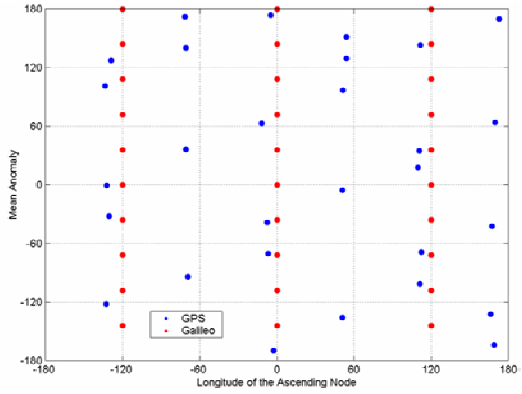

Figure 7 Simulated GPS/Galileo constellation

Error-addition simulation test

The first test with simulated data consists of artificially added errors on an 'error-free' simulation, where originally there are only errors with a magnitude of $\varepsilon_i \sim N(0,4^2)$ present. An error of the size of 25 m was inserted into 1, 2... 10 measurements (see implementation order and a skyplot of the first epoch of the test in Fig. 8) during an overall 7900-second simulation every 10-second-period creating overall 790 cases with each number of added errors. This test was conducted to assess the capability of detection and exclusion when inserting errors just above the MDB values of the measurements.

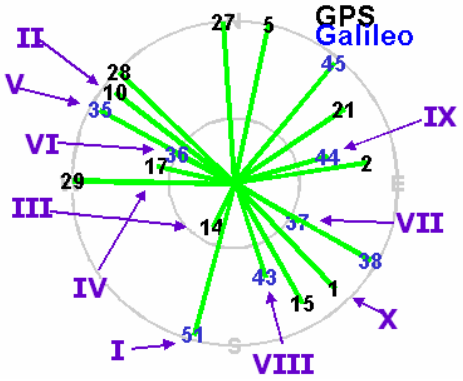

Figure 8 Skyplot of first epoch in simulation test {GPS denoted in black and Galileo denoted in blue}

Table 1 presents the detection and exclusion percentages of the artificial error-cases when the global test, 'FDE A', and 'FDE B' were applied (columns I, II, and III). Multiple errors make correct exclusion more difficult due to the assumption of a single error not holding, but detection is usually obtainable. In addition, the RMS of the 3D position errors of the 790 cases with each number of errors added are presented (the raw-case, and when the two different FDE schemes were applied) as well as the 1.56*MRSE (~95%) estimate of the accuracy of the position solutions. No subset testing was conducted due to the large amount of subsets to be assessed when GPS and Galileo measurements are both available.

Table 1 Results of the global test for detection and the FDE schemes for exclusion in error-cases

# of added errors	I (%)	II (%)	III (%)	IV [m]	V [m]	VI [m]	VII [m]
0	-	-	-	4.1	6.5	-	-
1	97	97	95	6.6	11.9	4.3	4.4
2	100	98	93	7.9	14.8	4.7	5.0
3	100	82	78	10.9	16.3	12.2	12.3
4	100	84	81	12.1	18.2	12.6	12.8
5	100	69	68	15.1	18.8	21.3	21.4
6	100	42	43	21.9	17.7	28.1	28.1
7	100	34	35	21.9	18.1	26.8	26.8
8	100	21	21	26.9	16.4	28.3	28.3
9	100	21	21	28.0	17.3	30.3	30.3
10	99	13	13	29.0	15.7	30.4	30.4

I:	% of correct detection with global test
II:	% of correct exclusion with 'FDE A'
III:	% of correct exclusion with 'FDE B'
IV:	RMS of raw 3D errors when errors added [m]
V:	RMS of 1.56*MRSE accuracy estimates [m]
VI:	RMS of 3D errors after 'FDE A' [m]
VII:	RMS of 3D errors after 'FDE B' [m]

The 1.56*MRSE provides a pessimistic estimate of the accuracy when up to five errors were implemented after which it becomes optimistic. The FDE schemes improve accuracy only in the cases with up to a couple of added errors. When the FDE procedures fail to exclude all of the erroneous measurements, still some errors are left, and depending on the geometry, the outcome is worse and associated with greater errors. False exclusions were also performed leaving thus erroneous measurements in the solution computation decreasing the accuracy. Failed exclusions are partly due to the small error in each measurement, only 25 m, which is just slightly over the MDB value of some of the measurements. With the high redundancy, the small errors tend to average out, also in the resulting residuals, making exclusion more difficult. Fig. 9 shows the RMS values of the number of exclusions in the error-cases with different amounts of added errors expressing the incapability of excluding enough erroneous measurements. The 'FDE A' procedure demonstrates slightly more exclusions. Fig. 10 presents the 3D error in the 790 error-cases when five errors were artificially added. The accuracy decreases, and the largest errors are due to false exclusions of good measurements leaving the erroneous. In some cases, the FDE schemes manage to improve accuracy by making correct exclusions.

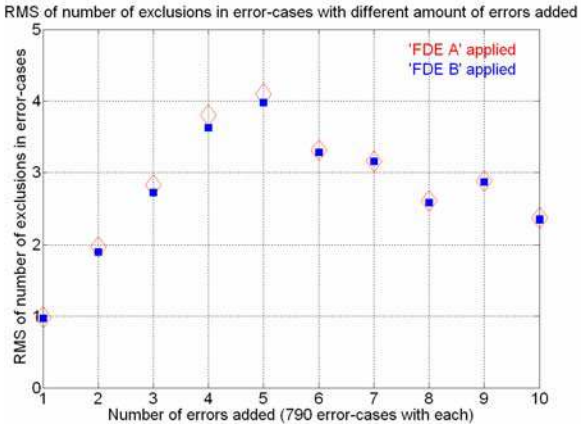

Figure 9 RMS of number of exclusions in error-cases

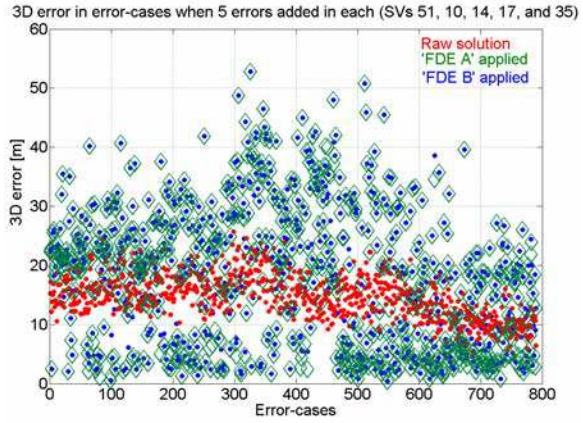

Figure 10 3D error in error-cases with 5 added errors

Degraded-measurement GPS/Galileo simulation test

A 6-hour GPS/Galileo simulation test with erroneous measurements of an urban environment was conducted. This test was performed to assess the capability of detection and exclusion when larger errors are present. Fig. 11 presents the range errors in this simulated data set and Fig. 12 the elevation angles for all the available satellites. Errors reach 150 m in this simulation and include randomly generated in-phase and out-of-phase multipath in six of the satellites in view, moderate ionosphere and troposphere errors, receiver noise, and orbital errors. As background information about the simulation, Fig. 13 presents the number of satellites in view and the PDOP values for the GNSS simulation scenario, and Fig. 14 presents the theoretical MDB (Eq. 6) and TPE (Eq. 9) maximum values for each epoch.

Figures 15, 16, 17, and 18 present the 3D position errors of the simulation test, the 1.56*MRSE (~95%) accuracy estimate, and the 3D error when 'FDE A' and 'FDE B' were applied, respectively. Statistics are provided in all the figures, and final global test failure indications are provided in the figures where the two FDE schemes were applied. The MRSE-based accuracy estimate provides a good approximation of the accuracy of the GPS/Galileo simulation. When applying the two FDE schemes, the maximum 3D error and the RMS values are decreased

improving thus the accuracy. Fig. 19 provides the PDOP values after 'FDE A' and 'FDE B' were performed and PDOP remain still excellent due to the high redundancy. Fig. 20 presents the number of exclusions when the FDE schemes were performed, and the 'FDE A' scheme demonstrates slightly more exclusions. The maximum 3D error values coincide to some extent with the slight degradation in PDOP, and they are caused by unsuccessful exclusion – false exclusion of good measurement leaving the erroneous.

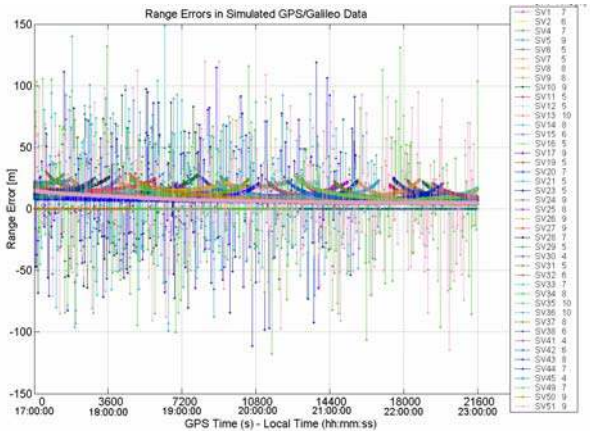

Figure 11 Range errors in the erroneous measurement simulation test with the software simulator

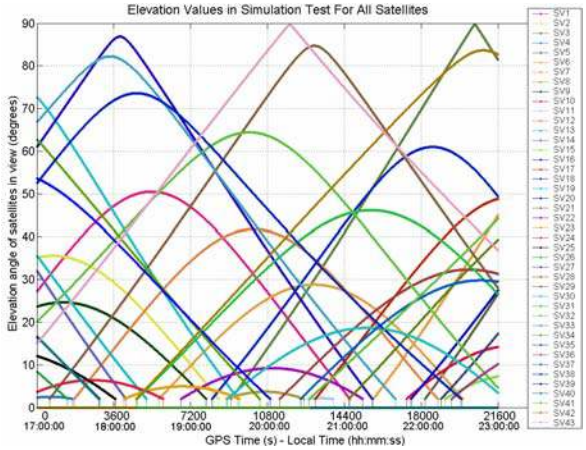

Figure 12 Elevation angles in simulation test

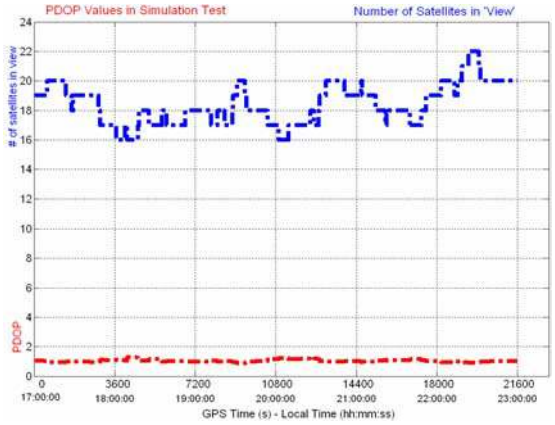

Figure 13 Number of satellites in view and PDOP values in simulation test

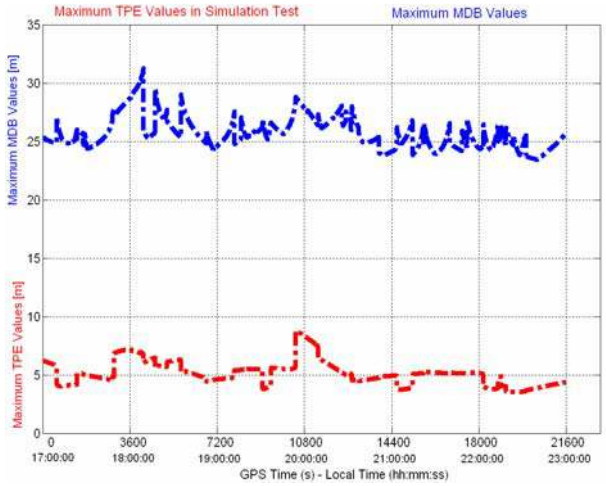

Figure 14 Maximum MDB and TPE values at each epoch in simulation test

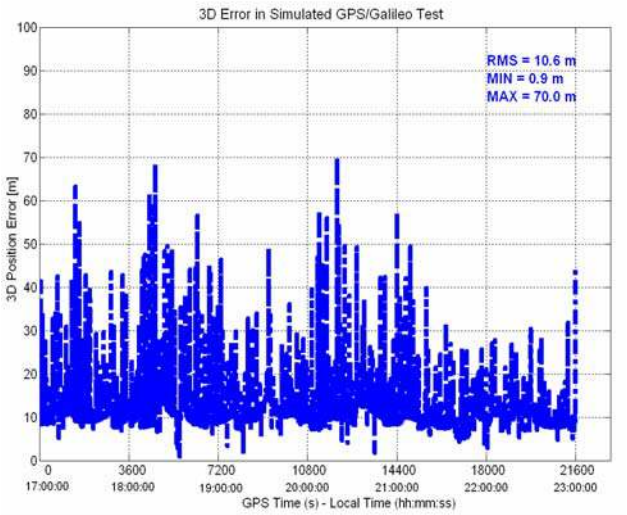

Figure 15 Raw least squares 3D position error in simulation test

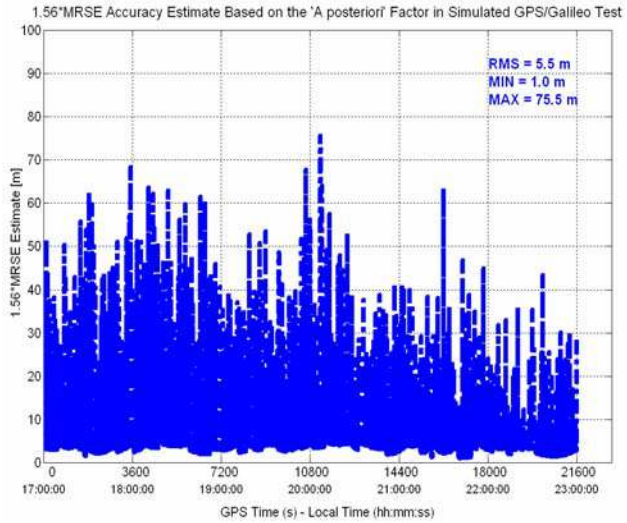

Figure 16 3D accuracy estimate (~95%) in simulation test

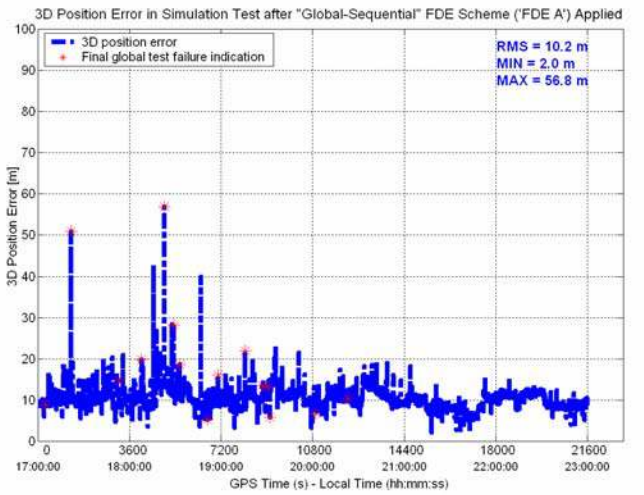

Figure 17 3D position error after 'FDE A' applied in simulation test

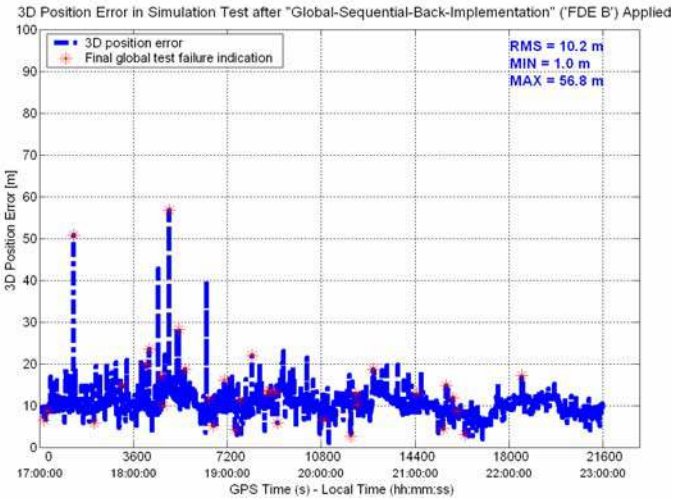

Figure 18 3D position error after 'FDE B' applied in simulation test

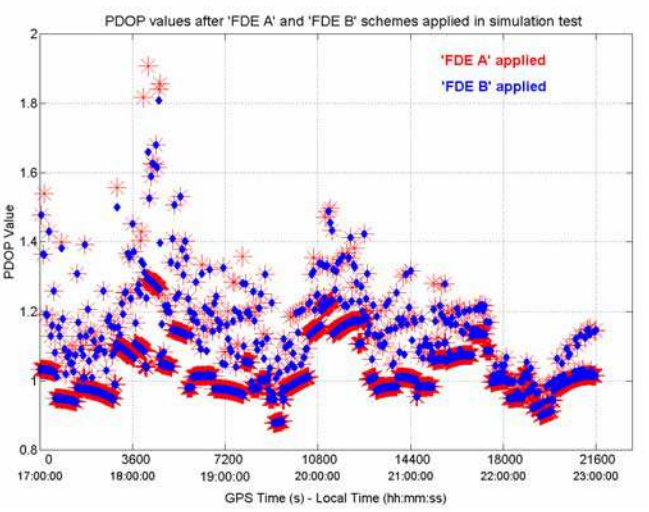

Figure 19 Resulting PDOP values when applying 'FDE A' and 'FDE B' in simulation test

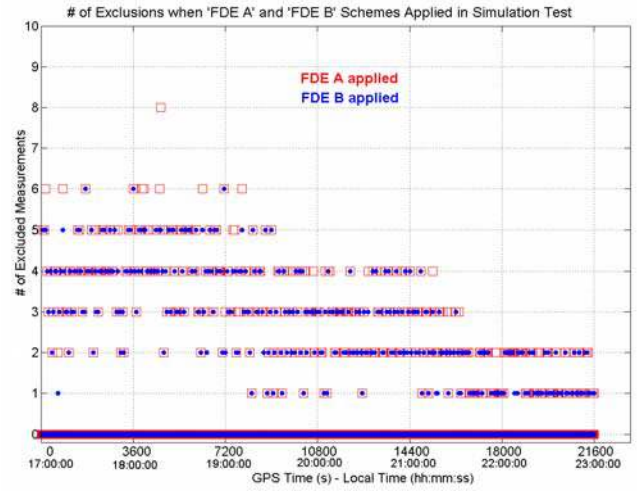

Figure 20 Number of exclusions when applying 'FDE A' and 'FDE B' in simulation test

INDOOR AND URBAN HIGH-SENSITIVITY GPS RELIABILITY TESTS

The theory of HSGPS (High-Sensitivity GPS) lies in the improved ability to acquire and track weak GPS signals (Lachapelle et al 2003, MacGougan et al 2002). The increased tracking capability of HSGPS is highly beneficial in terms of solution availability and increased redundancy for reliability of navigation. However, simultaneously, severe interference effects due to poor signal conditions of indoor and urban environments lead to large measurement errors. Reliability monitoring in terms of proper FDE becomes increasingly important in HSGPS for degraded environment positioning (Lachapelle et al 2003, Collin et al 2003).

Indoor and urban environment HGPS data was gathered to test the performance of the FDE schemes. An indoor test was performed as well as an urban environment pedestrian test both with a HSGPS (SiRF XTrac-LP™) receiver. First, a test was carried out inside a garage shown in Fig. 21 over a period of 12 hours in June 2003 (Lachapelle et al 2003). The differential mode was used to eliminate orbit and atmospheric errors.

Figure 21 Garage used in indoor test

Fig. 22 presents the estimated pseudorange errors (EPE) for the indoor garage data. The EPE values for each satellite were obtained by post-processing techniques

when knowing the reference position by surveying techniques. Since differential corrections were applied, the EPE is in this case a good estimate of the error caused by multipath and receiver noise. Figure 23 presents the number of satellites in view and HDOP values in the test.

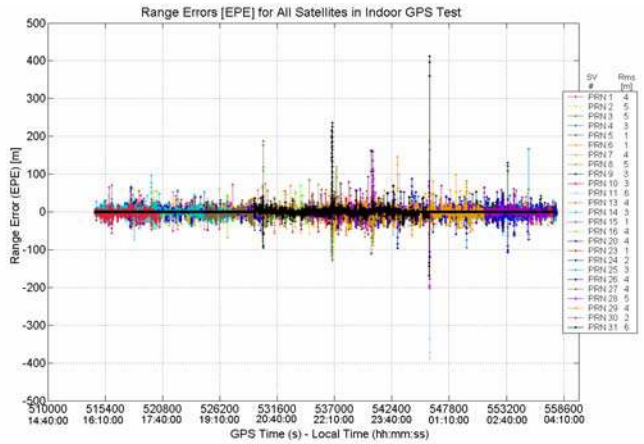

Figure 22 Estimated pseudorange errors (EPE) for all satellites during indoor test

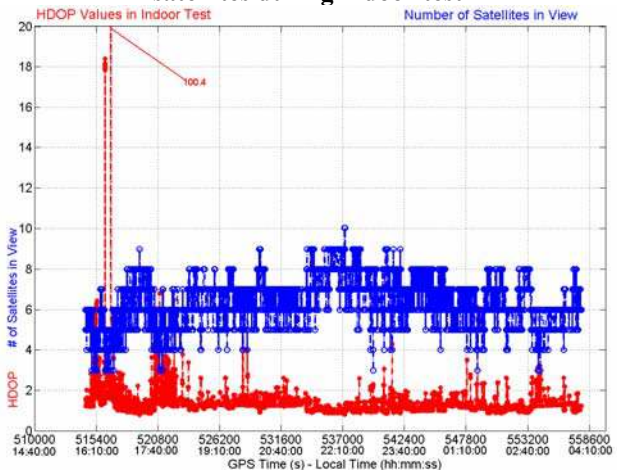

Figure 23 Number of satellites in view and HDOP values in indoor test

In processing the indoor data with epoch-by-epoch least-squares (a modified version of C^{3}NAVG^{2TM}), height constraining was always used to have the best obtainable redundancy. Fig. 24 presents the raw 2D least-squares position error of the indoor test, and Fig. 25 presents the 2D accuracy estimate, the 2*DRMS (~95-98%) estimate, for the indoor test providing a slightly pessimistic but reasonable approximation of the accuracy. Figures 26, 28, and 30 present the 2D errors when 'FDE A', 'FDE B', and subset testing were applied, respectively. Statistics of the errors are provided in all the figures. Figures 27, 29, and 31 present the 2D errors when applying the FDE schemes and a HDOP cut-off of the value 5. These figures include indications of points with not enough redundancy for RAIM, final global test failure indications in 'FDE A' and 'FDE B' cases (Figures 27 and 29), and subset testing failure indications in the subset testing FDE case (Fig. 31). The HDOP cut-off slightly decreases the overall availability but accuracy is obviously improved. The global test failure indications in the figures are not always justified, and sometimes failure indications are given to points where the overall error is not significant but the 'a posteriori' variance factor is just above the threshold value of the test. Some erroneous measurements are being excluded and others still remaining in the position computation making the test just about to fail and the errors however averaging out in the position.

Fig. 32 presents the HDOP values and Fig. 33 the number of exclusions after applying the different FDE schemes. The 'FDE A' scheme shows the most exclusions and thus the poorest HDOP values, and in general when the FDE schemes were applied, the maximum 2D errors coincide with the degraded HDOP values and the too many exclusions.

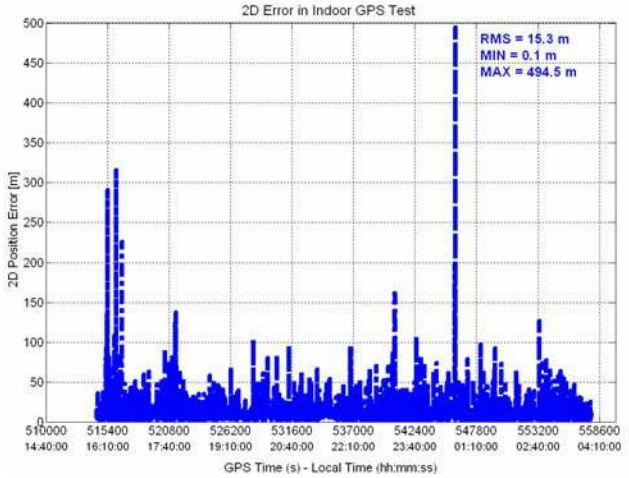

Figure 24 Raw 2D position error in indoor test

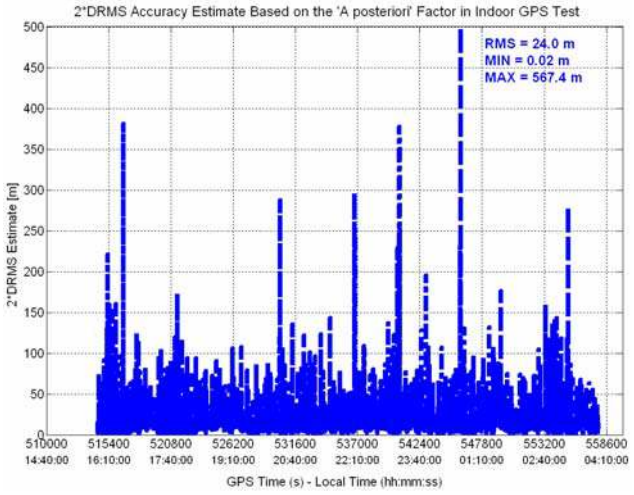

Figure 25 2D accuracy estimate (~95-98%) in indoor test

When applying the 'FDE A' scheme, results are poor, since both the RMS and maximum error values are increased (Fig. 26) due to exclusions of measurements too vital to the solution geometry as seen also in the figure describing the HDOP values after exclusions (Fig. 32).

However, when using the HDOP cut-off, accuracy is improved compared to the raw least squares solution. The back-implementation FDE process, 'FDE B', and the subset testing FDE improve the overall accuracy and provide good results, especially when using the HDOP cut-off. Some of the maximum peak errors remaining have failure indications or not enough redundancy present to conduct the consistency testing. The results show, however, the difficulty of implementing FDE methods for urban environments when redundancy is low and satellite geometry worsen when critical satellite measurements are removed.

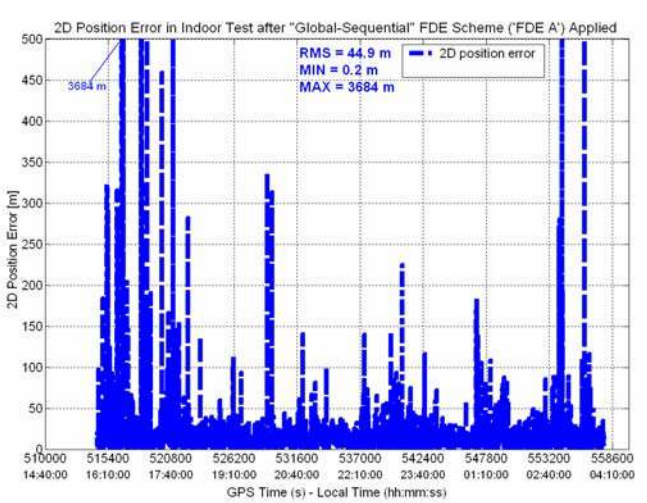

Figure 26 2D position error after 'FDE A' applied

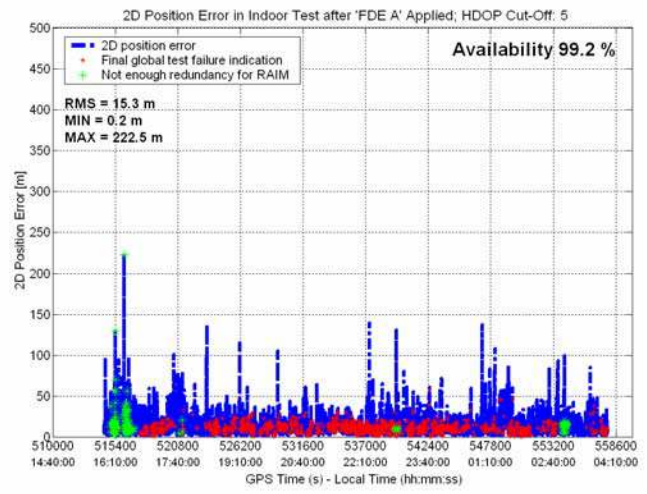

Figure 27 2D position error after 'FDE A' applied – HDOP Cut-Off: 5

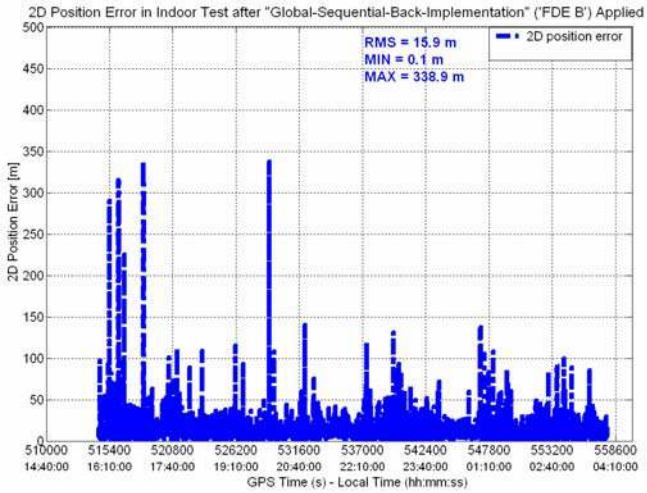

Figure 28 2D position error after 'FDE B' applied

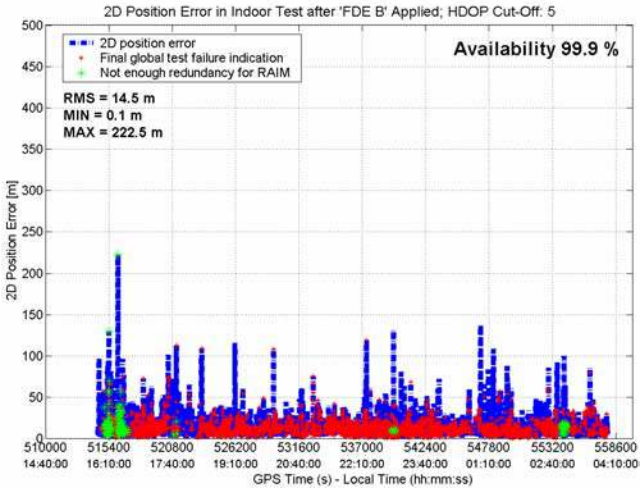

Figure 29 2D position error after 'FDE B' applied – HDOP Cut-Off: 5

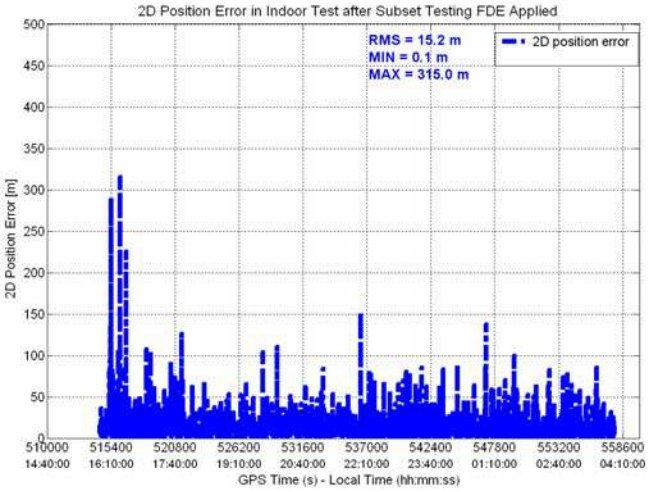

Figure 30 2D position error after subset testing FDE applied

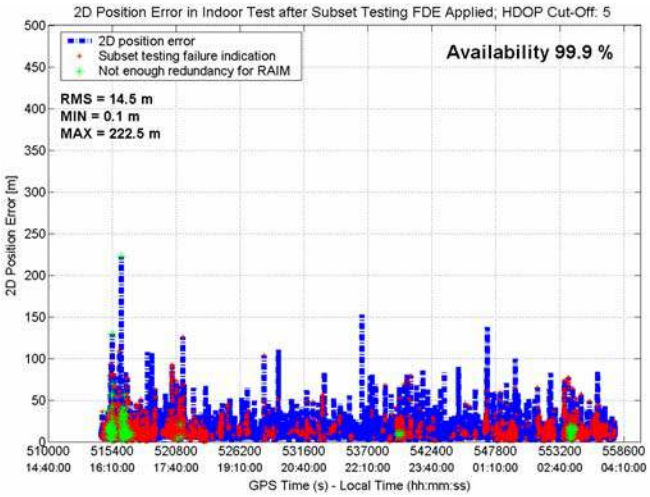

Figure 31 2D position error after subset testing FDE applied– HDOP Cut-Off: 5

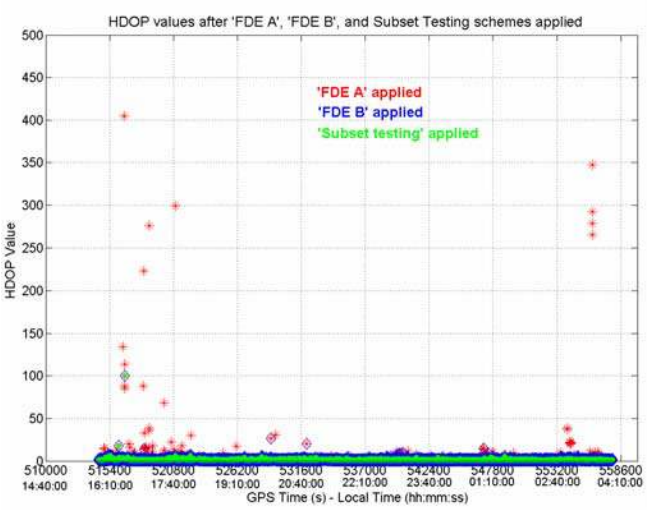

Figure 32 Resulting HDOP when applying 'FDE A' and 'FDE B', and the subset testing schemes

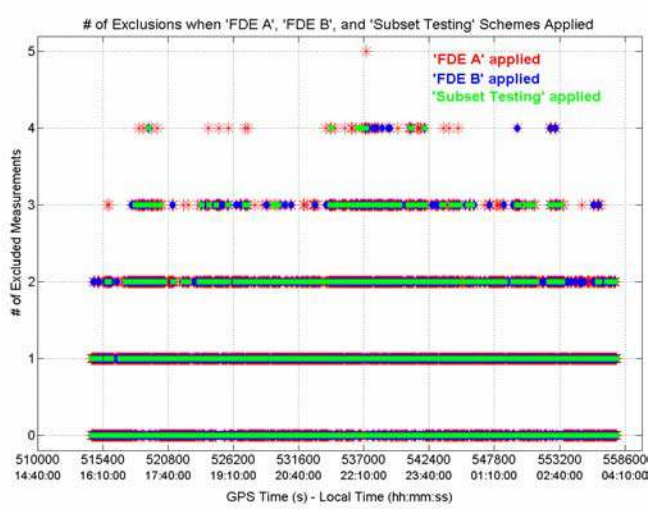

Figure 33 Number of exclusions when applying 'FDE A' and 'FDE B', and the subset testing schemes

A pedestrian test at the University of Calgary campus with the HSGPS receiver was performed in September 2003 including both open-sky and indoor sections (Collin et al 2003). The test trajectory is shown in Figure 34. The test starts in an open-sky parking lot after which the test person walks into a building, walks four loops indoors, and walks back to the parking lot. The red line in the trajectory figure indicates a building outline, the black line indicates a carrier-phase GPS reference outdoors, and the indoor portion of the conducted test is shown in grey. Figure 35 is a photo of the indoor area showing the two-floor concrete and glass building. In Fig. 36, the number of satellites in view and the HDOP values for the pedestrian test are shown including a gap in the obtained measurements beginning slightly after entering the building. In Fig. 37, the HSGPS positions from least squares processing without height constraining and utilizing the global consistency test for detection are presented. This figure shows how the solution accuracy degrades on approach to buildings due to reflected measurements, and further when indoors. In addition, it shows how the global test can assist to some extent identifying poor solutions and how some solutions lack the redundancy required for the consistency tests (n-$p \leq 0$).

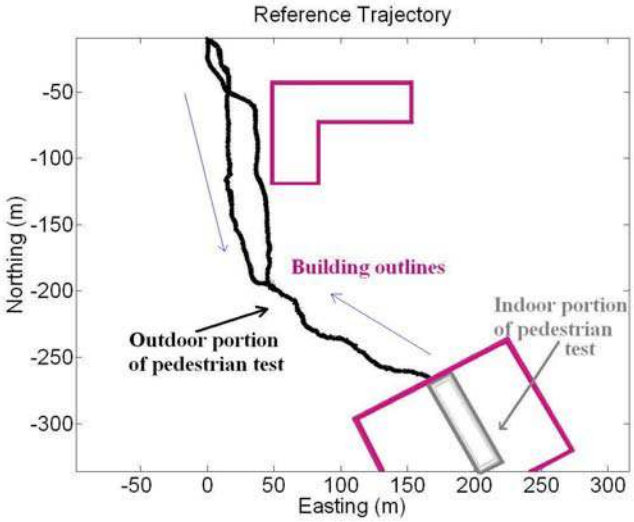

Figure 34 Reference trajectory in outdoor/indoor pedestrian test

Figure 35 Indoor portion of pedestrian test

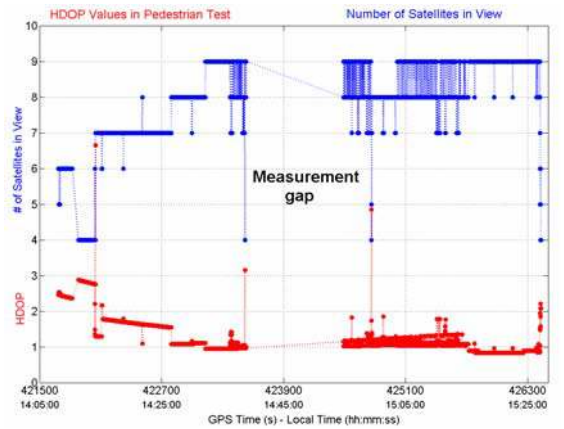

Figure 36 Number of satellites in view and HDOP

Figures 38, 39, and 40 present HSGPS position solutions including the partial reference trajectory outdoors when 'FDE A', 'FDE B', the subset testing FDE were applied, respectively. Fig 41 presents the resulting HDOP values after the different FDE schemes were applied. Fig. 42 presents the number of exclusions with the different FDE schemes indicating that 'FDE A' and subset testing FDE perform the most exclusions in the exclusion procedure.

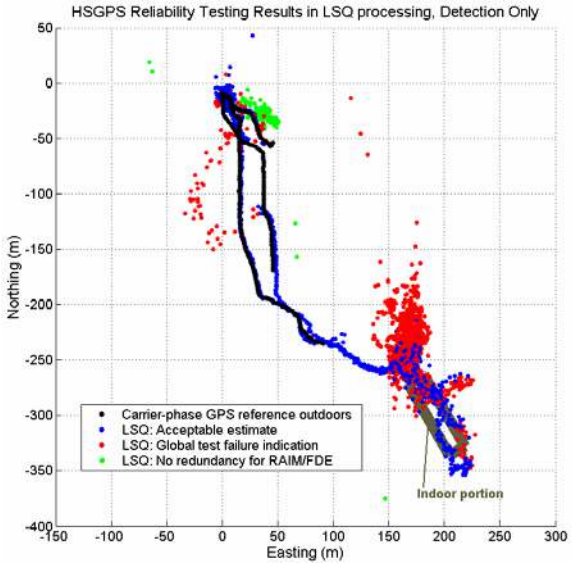

Figure 37 Pedestrian test in blue, with global test detection and no redundancy indications in red and green, respectively; Detection only

Indoors, HSGPS has good availability, but poor accuracy attached with the attenuated signals that are being tracked making reliability monitoring difficult. Namely, in the pedestrian test, some erroneous situations have not even been detected by the global test, especially while indoors, due to errors averaging out and the low redundancy. In addition, the FDE schemes do not increase reliability due to exclusions of only some erroneous measurements leaving still others. This leads only to a decrease in geometry (Fig. 41) and thus accuracy. However, the reliability warnings provided by the global test are still useful information.

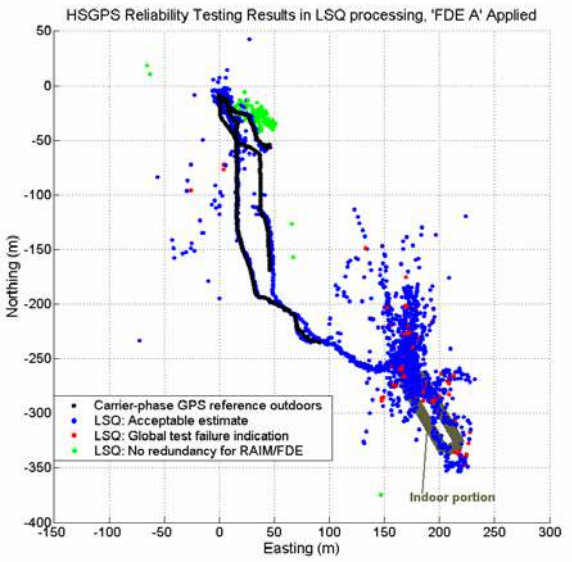

Figure 38 Pedestrian test in blue, with final global test detection and no redundancy indications in red and green, respectively; 'FDE A' applied

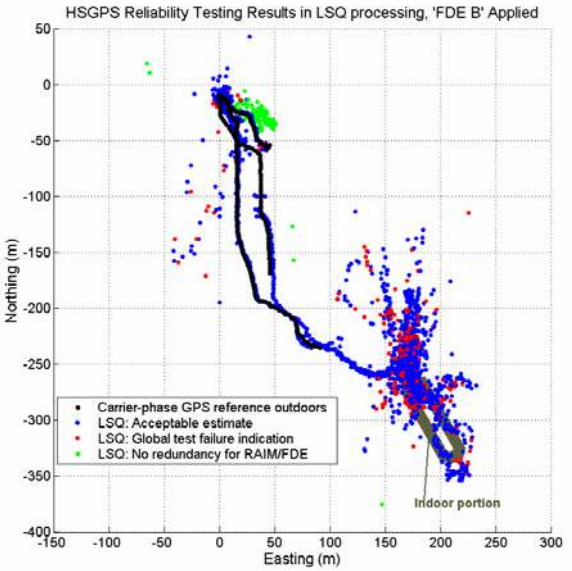

Figure 39 Pedestrian test in blue, with final global test detection and no redundancy indications in red and green, respectively; 'FDE B' applied

The assumption of the normally distributed zero-mean errors is ultimately incorrect due to the occurrence of multiple blunders caused by attenuation and cross-correlation effects on the signals tracked inside the building. In some cases, the errors cancel each other out to some extent making the test statistic, the 'a posteriori' variance factor, to stay within the predetermined limits of the global test. In some of the obvious failure situations, in the indoor HSGPS pedestrian case, the implemented RAIM and FDE results are not trustworthy due to the multiple blunders, but overall, RAIM provides essential information of the reliability of the least squares position solution, for example, to a sensor-system initialization.

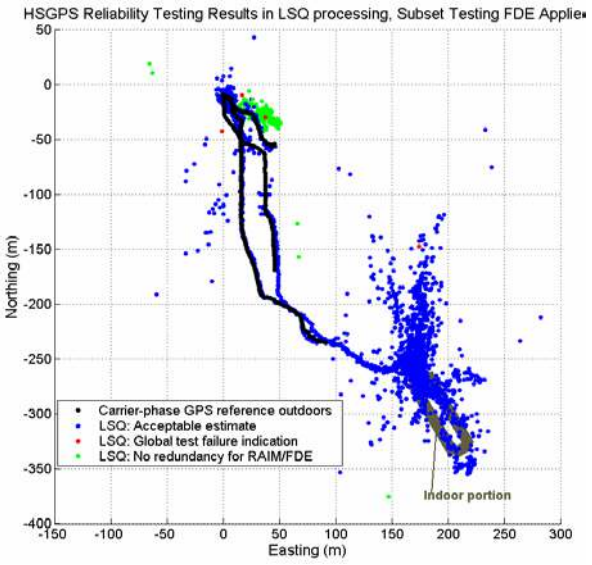

Figure 40 Pedestrian test in blue, with final global test detection and no redundancy indications in red and green, respectively; Subset testing FDE applied

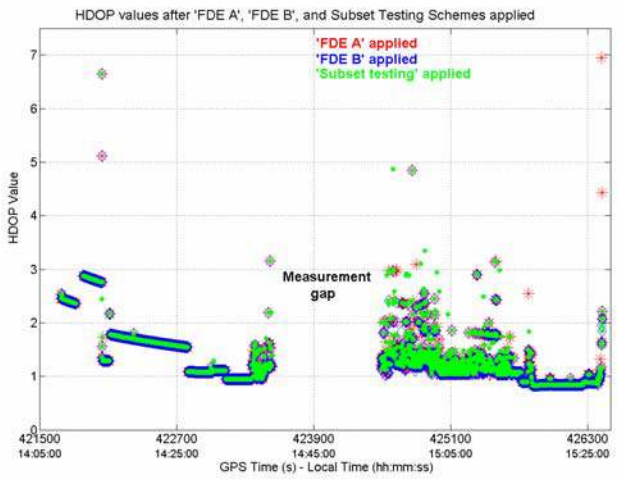

Figure 41 Resulting HDOP values when applying 'FDE A', 'FDE B', and the subset testing schemes

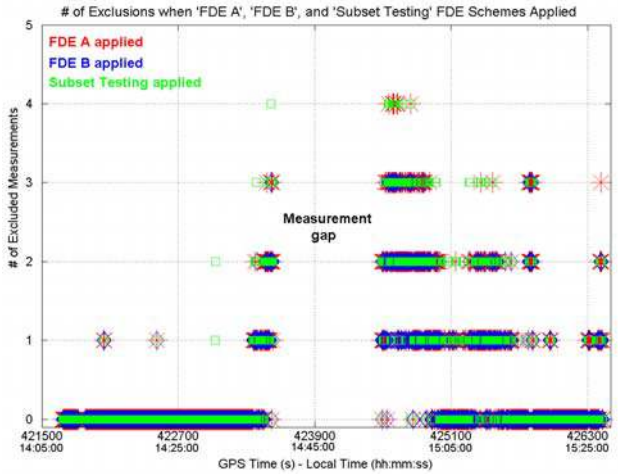

Figure 42 Number of exclusion when applying 'FDE A', 'FDE B', and the subset testing schemes

CONCLUSIONS

The paper discussed reliability monitoring schemes intended for poor signal-environment GNSS fault detection and exclusion, and presented some case studies with simulated GPS/Galileo and real HSGPS data. When assessing the reliability and accuracy performance of the implemented FDE schemes, it can be concluded that the FDE methods presented in this report are not perfect but eligible possibilities for degraded GNSS signal environment reliability analysis, particularly the 'FDE B' scheme and the subset testing, though subset testing is computationally heavy for integrated GPS/Galileo. Both of the methods require still some further analysis and optimization concerning, for example, the performance criteria. It can be stated that a GNSS FDE scheme for multiple blunder situations is an essential but a difficult problem to be studied due to the traditional assumptions of measurement errors not holding, and more analyses should be performed in order to obtain a reliable blunder detection and exclusion procedure. The presented accuracy estimation using the 'a posteriori' variance factor and the covariance matrix of the estimated unknown user coordinates to estimate the accuracy of the obtained GNSS position solution showed promising results in providing approximated accuracy information to the user.

Future work will include more analysis and testing of the reliability monitoring procedures with different environment scenarios, a supplemental GNSS RAIM/FDE scheme including velocity-domain residual monitoring, and analysis of the optimal performance criteria of the consistency tests for urban environments. The performance parameters need to be adaptive in order to be used in different location situations. In addition, the C/N_0 values should be taken into account in the FDE schemes by proper measurement weighting and in forming the accuracy estimates for degraded signal environments. Certain filtering when knowing the system dynamics and taking the geometry weakening more effectively into account prior to rejecting observations are also subjects of ongoing research. In this research, epoch-by-epoch least squares processing was used for analysis purposes but for real applications certain filtering approaches will become necessary.

ACKNOWLEDGMENTS

The authors would like to thank J. Collin, D. Dao, O. Mezentsev, Dr. A. Wieser, and the PLAN group at the University of Calgary for assistance. In addition, acknowledgements are given to Tampere University of Technology, Finland, and the Nokia Foundation for support, and to SiRF Technologies, Inc., San Jose, CA, for providing test equipment. This work was partly funded by the Auto 21 Network of Centres of Excellence.

REFERENCES

Alves P., The effect of Galileo on Carrier Phase Ambiguity Resolution, ION GPS 2001, Salt Lake City, UT, USA, September 11-14, 2001, pp. 2086-2095.

Baarda W., A testing procedure for use in geodetic networks, Netherlands Geodetic Commission, Publication on Geodesy, New Series 2, 5, Delft, Netherlands, 1968.

Brown R.G., A baseline RAIM scheme and a note on the equivalence of three RAIM methods, ION NTM 1992, San Diego, CA, USA, January 27-29, 1992, pp. 127-138.

Caspary W.F., Concepts of Network and Deformation Analysis, UNSW, Australia, School of Surveying, Monograph, 11, 1988.

Collin J., H. Kuusniemi, O. Mezentsev, G. Lachapelle, HSGPS under Heavy Signal Masking - Accuracy and Availability Analysis, NORNA 2003 Conference, Nordic Institute of Navigation, M/S Mariella, Stockholm-Helsinki-Stockholm, 2-4 December, 2003, 11 p.

Gertler J.J., Fault Detection and Diagnosis in Engineering Systems, Marcel Dekker Inc., 1998, 484 p.

Hawkins D.M., Identification of Outliers, Chapman & Hall, London/New York, 188 p.

E.D. Kaplan (ed.), Understanding GPS: Principles and Applications, Artech House Inc., 1996, 554 p.

Kelly R.J., The Linear Model, RNP, and the Near-Optimum Fault Detection and Exclusion Algorithm, invited paper in Papers published in NAVIGATION, Volume V, Institute of Navigation, 1998, pp. 227-259.

Kuang S., Geodetic Network Analysis and Optimal Design, AnnArbor Press, Chelsea, Michigan, 1996, 368 p.

Lachapelle G., H. Kuusniemi, D.T.H. Dao, G. MacGougan, M.E. Cannon, HSGPS Signal Analysis and Performance under Various Indoor Conditions, ION GPS 2003 Conference, Portland, Oregon, USA, 9-12 September, 2003, pp. 1171-1184.

Leick A., GPS Satellite Surveying, John Wiley & Sons Inc., second edition, 560 p.

Lu G., Quality Control for Differential Kinematic GPS Positioning, Master's thesis, University of Calgary, UCGE Report 20042, 1991, 103 p.

Luo N., G. Lachapelle, Relative Positioning of Multiple Moving Platforms Using GPS, IEEE Transactions on Aerospace and Electronic Systems, Vol. 39, No. 3, July 2003, pp. 936-948.

MacGougan, G., G. Lachapelle, R. Klukas, K. Siu, L. Garin, J. Shewfelt, and G. Cox, Performance Analysis of A Stand-Alone High Sensitivity Receiver, GPS Solutions, Springer Verlag, 6, 3, 2002, pp. 179-195.

Malicorne M., M. Bousquet, and V. Calmettes, Galileo Performance Improvement for Urban Users, ION GPS 2001, Salt Lake City, UT, USA, September 11-14, 2001, pp. 2105-2113.

Ober P.B., Integrity Prediction and Monitoring of Navigation Systems, Ph.D. thesis, Delft University of Technology, The Netherlands, Integricom Publishers, 2003, 146 p.

O'Keefe K., Availability and Reliability Advantages of GPS/Galileo Integration", ION GPS 2001, Salt Lake City, USA, Sept. 11-14, 2001, pp. 2096-2105.

Parkinson B.W. (ed.), J.J Spilker (ed.), Global Positioning System: Theory and Applications, Volume 1 and 2, AIAA Inc., 1996, 793 p. and 643 p.

Petovello M.G., Real-Time Integration of a Tactical-Grade IMU and GPS for High-Accuracy Positioning and Navigation, Ph.D. thesis, The University of Calgary, UCGE Report 20173, 2003, 242 p.

Romay Merino M.M., A.J. Gavín Alarcón, I. Juárez Villares, E. Herráiz Monseco, An Integrated GNSS Concept, Galileo & GPS, benefits in terms of Accuracy, Integrity, Availability and Continuity, ION GPS 2001, Salt Lake City, UT, USA, September 11-14, 2001, pp. 2114-2125.

Ryan S., G. Lachapelle, Impact of GPS/Galileo Integration on Marine Navigation, ION AM 2000, San Diego, CA, USA, June 26-28, 2000, pp. 721-732.

Ryan S., Augmentation of DGPS for Marine Navigation, Ph.D. thesis, The University of Calgary, UCGE Report 20164, 2002, 248 p.

Teunissen P.J.G., Quality Control and GPS, Chapter 7 in GPS for Geodesy, 2nd Edition, ed. P.J.G. Teunissen and A. Kleusberg, Springer, New York, NY, 1998.

Van Graas F., J.L. Farrell, Baseline Fault Detection and Exclusion Algorithm, ION AM 1993, Cambridge, MA, USA, June 21-23, 1993, pp. 413-420.

Weber T., H.L. Trautenberg, C. Schäfer, GALILEO System Architecture – Status and Concepts, ION GPS 2001, Salt Lake City, UT, USA, September 11-14, 2001, pp. 1264-1273.

Wieser A., Robust and fuzzy techniques for parameter estimation and quality assessment in GPS. Ph.D. Thesis, TU Graz, 2001, 253 p.